Multi-compartment spatiotemporal metabolic modeling of the chicken gut guides the design of dietary interventions

Irina Utkina[1], Mohammadali Alizadeh[2], Shayan Sharif[2], John Parkinson[1,3,*]

[1] Program in Molecular Medicine, Hospital for Sick Children, Toronto, Ontario, Canada

[2] Department of Pathobiology, Ontario Veterinary College, University of Guelph, Guelph, Ontario, Canada

[3] Department of Biochemistry, University of Toronto, Toronto ON, Canada

[*] Contact information for the Corresponding Author:

Program in Molecular Medicine, The Hospital for Sick Children, Toronto, ON, Canada M5G 0A4

jparkin@sickkids.ca

Keywords: Microbiome; Metabolic Modeling; Poultry Gut; Dietary Interventions; Metabolic Interactions

ABSTRACT

Understanding the interactions between diet and the gut microbiome is critical for identifying dietary interventions that support gut health. This is of particular importance for poultry where the elimination of antibiotic growth promoters has resulted in an alarming rise in enteric infections with significant economic consequences. While the application of computational models capable of dissecting the metabolic interactions supporting gut communities has shown promise, they remain limited, largely ignoring the physiological and geographical considerations of the poultry gastrointestinal tract. To address these limitations, we developed the first multi-compartment, spatiotemporally-resolved metabolic model of the chicken gastrointestinal tract. Our six-compartment framework integrates avian-specific physiological features including bidirectional flow, feeding-fasting cycles, and compartment-specific environmental parameters. The model captured distinct metabolic specialization along the gut, with upper compartments enriched for biosynthetic pathways and lower compartments specialized for fermentation. *In silico* screening of 34 dietary supplements revealed context-dependent metabolic responses and predicted cellulose, starch, and L-threonine as robust enhancers of short-chain fatty acid production. A controlled feeding trial validated key predictions, particularly for butyrate, with prediction accuracy further improved through integration of trial-specific microbial community data. Our findings demonstrate that community composition is a major driver of metabolic outcomes and underscore the need for context-specific modeling. Our framework provides a mechanistic platform for rational dietary intervention design and is broadly adaptable to other animal or human gastrointestinal systems.

INTRODUCTION

Over the past eight decades, antibiotic growth promoters (AGPs) have played an important role in livestock production, promoting gut health and reducing the burden of infectious disease[1]. However, the rise of antimicrobial resistance (AMR) associated with the use of AGPs (with AMR hotspots persisting across major poultry-producing regions in Asia, South America, and North America[2]) has created an urgent need for efficacious alternatives[3,45,62]. Research efforts have identified several promising alternatives, including phytochemicals, organic acids, probiotics, and prebiotics[3,4]. However, these interventions produce inconsistent outcomes across production systems, with substantial variability in efficacy between studies and farms[3–5]. This inconsistency reflects a critical challenge: intervention efficacy depends on baseline conditions, including diet composition, microbiota structure, and host physiology[5]. Consequently, identification of effective alternatives requires a more complete understanding of how potential interventions interact in the context with these additional factors.

At the core of these relationships are the metabolic interactions between gut microbiota, responsible for the degradation of dietary components and provision of nutrients, both to the microbial community as well as the host. Helping dissect these relationships are frameworks such as constraint-based metabolic models capable of explicitly simulating biochemical reaction networks. Recent advances have scaled these models from single species to community-scale frameworks capable of capturing interspecies interactions and metabolite exchange[6,7]. Tools such as MICOM and BacArena now enable quantitative simulations of microbiome metabolism under dietary perturbations[8–10]. In humans, these approaches have accurately predicted individual short-chain fatty acid (SCFA; metabolites associated with gut health[11]) profiles and revealed mechanistic links between microbial metabolism, host physiology, and diet[12,13]. Multi-compartment and agent-based frameworks have been established for mammalian systems, capturing pH gradients, oxygen diffusion, motility, and absorption along the gastrointestinal tract (GIT)[9,14–18]. Further, studies involving these platforms have shown that modeling the spatial organization of microbial communities improves predictive accuracy for metabolite fluxes and dietary intervention outcomes[14,16,17].

Despite the limited application of community metabolic modeling to livestock, initial studies have shown much promise, revealing the impact of keystone taxa, as well as AGPs and their potential alternatives[19–21]. A significant limitation in these models, however, has been the focus

on a single compartment, typically the ceca. Such models neglect the potential contributions of other compartments that feature distinct physical and chemical environments. Consequently, they do not capture the progressive processing of dietary components as they transit the GIT, or the functional contributions of individual taxa that may vary across sites – a limitation that is particularly relevant in the search for health-promoting probiotics that may colonize different regions[22,23]. The omission of these features impacts predictive accuracy for interventions affecting multiple gut sites and underscore the need for physiologically grounded, multi-compartment frameworks.

To address these limitations, we developed the first multi-compartment, spatiotemporally resolved metabolic model of the chicken GIT. Our six-compartment framework (gizzard, duodenum, jejunum, ileum, cecum, colon) integrates avian-specific physiological features, including bidirectional flow through peristalsis and reverse peristalsis, feeding-fasting cycles with diurnal shifts in gut motility, compartment-specific environmental parameters (pH, oxygen gradients, transit times), and nutrient absorption by the host. To reflect realistic variation in poultry production systems, the model was parameterized using 16S rRNA sequence survey data from chickens fed corn- or wheat-based diets, two nutritionally distinct formulations known to drive markedly different gut community structures and fermentative outputs[24–26]. The framework captured compartment-specific metabolic profiles, taxon-specific SCFA production, and temporal metabolite dynamics across feeding cycles. Systematic screening of 34 dietary supplements revealed context-dependent metabolic responses shaped by microbial community composition and gut region and identified cellulose, starch, and L-threonine as robust enhancers of SCFA production in the lower GIT. A controlled feeding trial provided direct experimental validation, with the accurate prediction of butyrate production. We further show that prediction accuracy increases with the use of community compositions representative of the birds being tested, that we suggest should be a prerequisite for developing precision nutrition strategies. Overall, our framework provides a mechanistic platform for rational design of dietary interventions to replace AGPs and advance strategies for sustainable poultry production.

RESULTS

Multi-compartment framework enables spatially resolved metabolic modeling

Previous metabolic models of chicken gut microbiomes have focused exclusively on cecal metabolism, neglecting how community composition varies across gut regions and how dietary nutrients are sequentially transformed during transit. To address these limitations, we developed a six-compartment model predicting both taxon-specific metabolic contributions and the fate of dietary inputs along the gastrointestinal tract. This framework connects adjacent gut sections, spanning from gizzard to colon, allowing the flow of both microbes and metabolites, and incorporates host physiological features including pH, oxygen gradients, motility, enzymatic digestion, and nutrient absorption.

Microbial community models for each compartment were built using 16S rRNA profiles from 10-day-old chickens fed either corn- (n=5) or wheat-based (n=5) diets. For each compartment, we selected representative taxa by identifying the most abundant bacterial families (comprising >1% relative abundance) and choosing the dominant taxa (represented as distinct Amplicon Sequence Variants (ASVs)) within those families that were mapped to high-quality chicken gut-derived MAGs[27–29]. Taxon selection was further informed by two additional criteria: documented prevalence in poultry microbiome literature and transcriptional activity in metatranscriptomic data from the same trial[5]. Genome-scale metabolic models for the resulting 29 bacterial taxa representing the core microbiota across compartments were reconstructed with gapseq[30]. To ensure the inclusion of key fiber-degrading pathways, models were additionally curated with carbohydrate-active enzymes derived from CAZyme predictions.

To account for physiological differences between gut sections, compartment-specific parameters such as pH, oxygen levels, and bacterial population sizes were set to reflect previously reported gradients along the tract (**Figure 1B**; see Methods). Nutritional inputs were calibrated to average daily feed intake and bacterial density, with feeding intervals matching poultry husbandry regimes (see Supplementary Methods). Transit of material (metabolites and taxa) between compartments was defined with reference to previous studies[31,32]. Nighttime dynamics, including reverse peristalsis, were simulated to mimic the fasted state and the reintroduction of digesta into the upper compartments. Finally, host-driven digestion and absorption of fatty acids, amino acids, and simple sugars were incorporated, with fractions removed from the relevant sections to reflect host uptake. Together, the developed

comprehensive *in silico* framework provides a spatially and temporally resolved representation of microbial community dynamics in the chicken GIT.

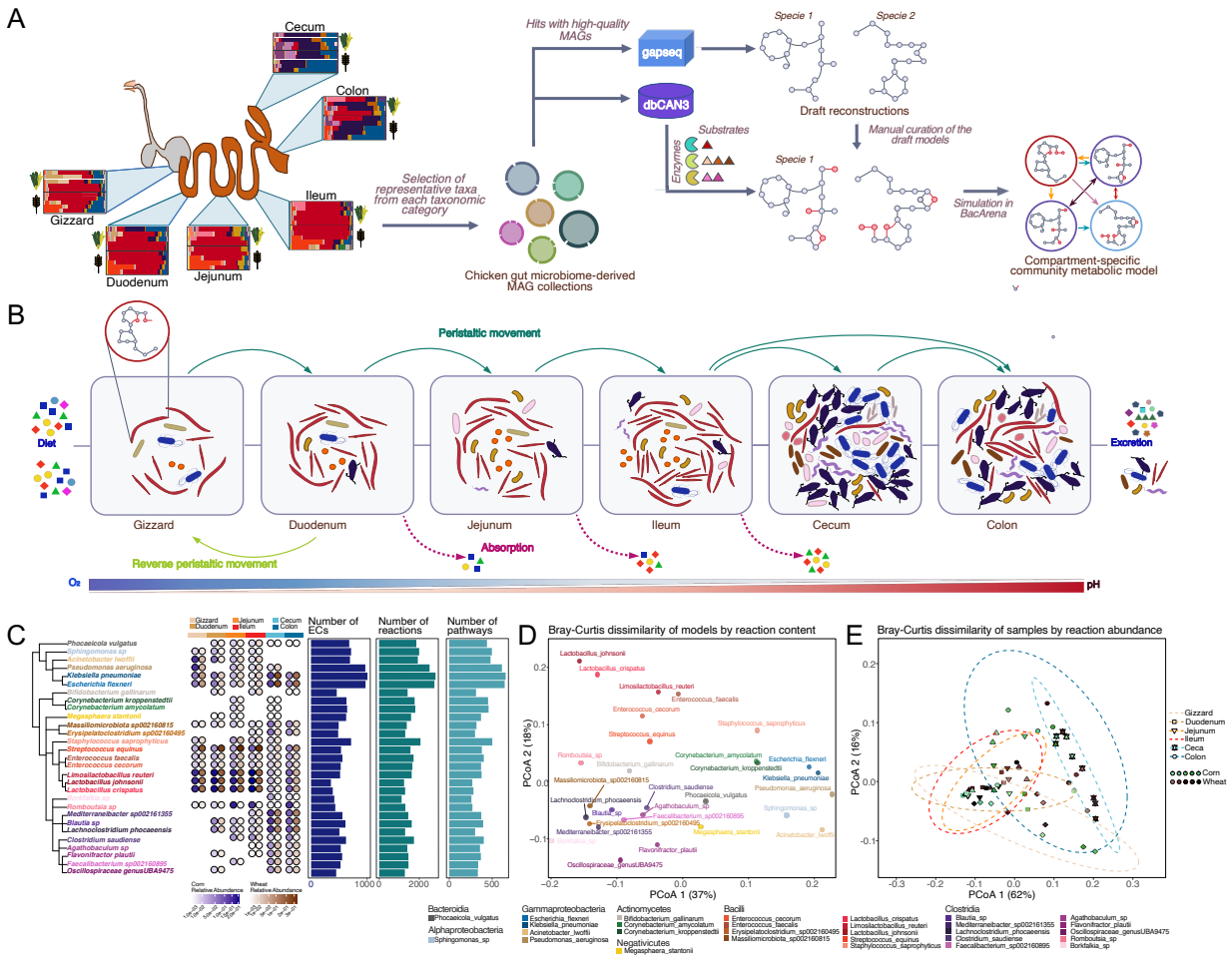

Figure 1.A. Overview of the modeling workflow. Community composition in each gut section (gizzard, duodenum, jejunum, ileum, cecum, colon) was parameterized using 16S rRNA profiles from corn- and wheat-fed chickens. Representative taxa were mapped to high-quality chicken gut-derived MAGs and reconstructed into genome-scale metabolic models with gapseq. Models were curated with CAZyme predictions (dbCAN3) to ensure representation of fiber-degrading pathways and integrated into sample- and compartment-specific community metabolic models. **B.** The six compartments are connected to simulate the flow of microbes and metabolites along the tract, with host physiological parameters including pH, oxygen, motility, digestion, and absorption incorporated to reflect site-specific conditions. **C.** Representative taxa selected to comprise core microbiota, shown in a phylogenetic tree with compartment-specific relative abundances (averaged across 10 samples) and the metabolic breadth of each corresponding GEM (number of EC numbers, reactions, pathways). **D.** PCoA of model reaction content using Bray-Curtis dissimilarity, illustrating clustering of taxa by their predicted metabolic repertoires. Each dot corresponds to a model of the taxon labeled. **E.** PCoA of reaction abundance profiles at the sample level, weighted by relative taxon abundance, showing clear separation of communities by gut compartment and partial separation by diet.

Compartment-specific metabolic capabilities reveal distinct functional specialization along the chicken GIT

155 The 29 selected taxa span diverse phylogenetic groups and metabolic capabilities, with
156 compartment-specific abundances reflecting the selective pressures of each gut region (**Figure**
157 **1C**). Metabolic capacities varied substantially across taxa: Enterobacteriaceae and other
158 metabolic generalists (taxa with large, broadly distributed repertoires) encoded the highest
159 numbers of reactions and pathways, while obligate anaerobes such as Oscillospiraceae
160 displayed more specialized repertoires, reflecting adaptation to fiber fermentation in the lower
161 gut. PCoA of enzyme content revealed clear metabolic stratification among the reconstructed
162 models (**Figure 1D**). Metabolic generalists (*Escherichia, Klebsiella, Pseudomonas*) were
163 separated from fermentation specialists (members of Lachnospiraceae and Oscillospiraceae
164 families), with *Lactobacillus* species forming an isolated cluster likely reflecting their
165 specialized fermentative metabolism. Notably, *Streptococcus* and *Romboutsia*, despite
166 showing diet-dependent prevalence patterns in upper GIT compartments, clustered closely
167 together, indicating metabolic similarity in the oxygenated, nutrient-rich upper gut. This
168 suggests that taxonomic shifts driven by diet do not necessarily translate to functional
169 divergence in the upper GIT communities. This contrasts with lower GIT communities, where
170 taxonomic differences between corn- and wheat-fed birds (Lachnospiraceae/Clostridiaceae
171 versus Enterobacteriaceae dominance) corresponded to distinct metabolic profiles.
172
173 Enzyme-level analysis further highlighted taxon-specific metabolic niches (**Figure S2**).
174 Obligate anaerobes restricted to lower GIT compartments (members of Ruminococcaceae,
175 Oscillospiraceae and Erysipelotrichaceae) encoded limited enzyme repertoires (510±62 ECs)
176 concentrated in glycan metabolism pathways (331±44 pathways), consistent with
177 specialization in cecal and colonic polysaccharide fermentation. By contrast, facultative
178 anaerobes present throughout the GIT including cecum and colon (Enterobacteriaceae,
179 *Pseudomonas*, and *Acinetobacter*) encoded substantially larger enzyme repertoires (913±145
180 ECs) spanning diverse metabolic pathways (600±81 pathways), reflecting their capacity as
181 metabolic generalists. Their presence in the lower GIT likely supports obligate anaerobes
182 through oxygen consumption and diverse metabolite production. Upper GIT-associated
183 facultative anaerobes (*Streptococcus*, *Romboutsia*, *Lactobacillus*) encoded intermediate
184 metabolic repertoires (505±114 ECs, 357±80 pathways), reflecting adaptation to rapidly
185 available nutrients in the upper gut. Certain taxa, including *Sphingomonas*, *Acinetobacter*, and
186 *Klebsiella*, uniquely possessed enzymes linked to xenobiotic degradation, suggesting
187 ecological roles in processing dietary or environmental compounds that other members of the
188 gut microbiome are unable to metabolize.

At the community level, PCoA based on reaction abundances revealed distinct clustering patterns that highlight metabolic specialization along the chicken gastrointestinal tract (**Figure 1E**). Although the metabolic profiles of the microbial communities differed significantly across gut compartments (PERMANOVA p=0.001), the pairwise differences between compartments were less pronounced (TukeyHSD p>0.05). The primary separation (PC1) distinguished upper from lower GIT communities based on contrasting metabolic strategies (**Figure S3A**). Upper GIT compartments were specifically enriched for bile salt hydrolases (glycocholate, glycochenodeoxycholate, taurodeoxycholate amidohydrolases), membrane lipid synthesis pathways (phosphatidate phosphatase, glycerol-3-phosphate cytidylyltransferase), and fatty acid biosynthesis (acetyl-CoA carboxylase), consistent with rapid biosynthetic activity in nutrient-rich, oxygen-replete conditions (**Figure S3B**). In contrast, cecal and colonic communities formed distinct clusters driven by enrichment in anaerobic fermentation pathways. Key metabolic specializations included SCFA synthesis (butyryl-CoA dehydrogenase, 3-hydroxybutanoyl-CoA oxidoreductase, butanoyl-CoA phosphotransferase for butyrate and propionate production), polysaccharide degradation (galacturonan hydrolases, arabinofuranosidases), and amino acid fermentation. The colon's metabolic profiles partially overlapped with upper GIT profiles, reflecting the direct anatomical linkage between the ileum and colon, enabling the gradual transition in microbial activity and community composition as the digesta moves from the small to the large intestine (**Figure 1E**).

Temporal dynamics of metabolite concentrations reveal compartment-specific signatures

Model simulations predicted taxon-specific SCFA production patterns that align with known metabolic capabilities (**Figure 2A**). *Escherichia flexneri* and *Klebsiella pneumoniae*, along with representatives of Lachnospiraceae and Erysipelotrichaceae families, were predicted to be among the major contributors to acetate production in the ileum, cecum, and colon. Acetate consumption by *Faecalibacterium* and *Clostridium* spp. fueled butyrate production[33,34], while *Streptococci,* particularly abundant in wheat-fed birds, displayed metabolic flexibility, producing acetate in the more oxygenated ileal environment but consuming it under anaerobic, glucose-scarce conditions in the cecum and colon. Such shifts align with experimental evidence for environment-dependent regulation of Streptococcal acetate metabolism[35–38]. *Bacteroides* species emerged as the primary propionate producers in the lower GIT, corroborating the well-documented capacities of this genus[39](**Figure 2A**). Together, these findings demonstrate that

the six-compartment model captures both taxon-level metabolic repertoires and community-level metabolic specialization, including the adaptation of microbial metabolism to the varying physiological conditions of different gut sections and reliable prediction of SCFA production, consistent with previous reports.

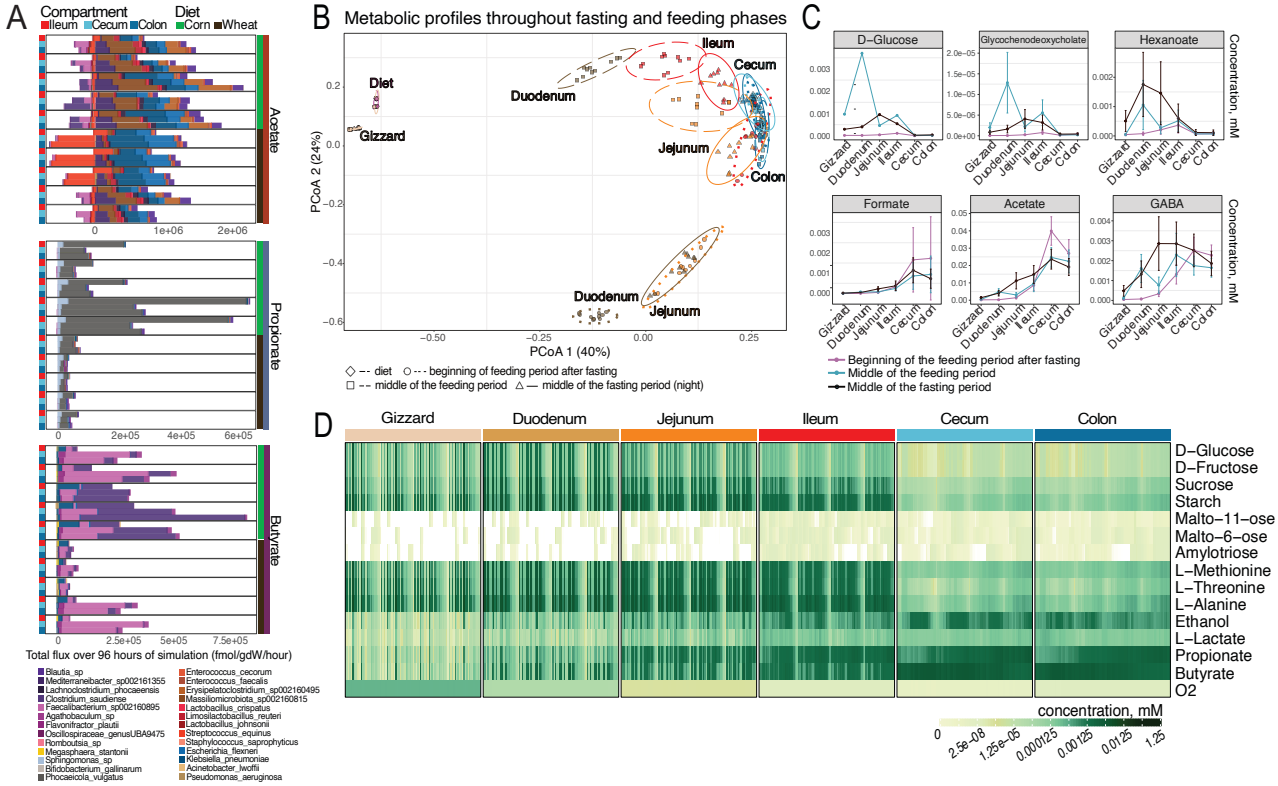

Figure 2. Temporal dynamics of metabolite concentrations across the chicken gastrointestinal tract during feeding and fasting cycles. A. Taxon-specific flux predictions for SCFAs over 96-hour simulations. **B.** Principal Coordinate Analysis (PCoA) of metabolite profiles across six gut compartments (gizzard, duodenum, jejunum, ileum, cecum, colon) at three time points: beginning of the feeding period after fasting, middle of the feeding period, and middle of the fasting period. Points are color-coded by compartment (corn- and wheat-fed samples combined to emphasize conserved compartment-specific signatures), with distinct clusters reflecting compartment-specific metabolic activities and shifts over time across both diets. **C.** Concentration profiles of selected metabolites across gut compartments at three time points: beginning of the feeding period (pink), middle of the feeding period (light blue), and middle of the fasting period (dark brown). The plots indicate the mean concentrations and standard deviations of metabolite concentrations from samples corresponding to chickens fed corn-based diet (n=5). **D.** Dynamics of metabolite concentrations across gut compartments during 96 hours of simulation for a selection of metabolites. Rows represent specific metabolites, with color intensity indicating concentration levels. The results shown were retrieved from simulation of one of the samples from corn-fed chicken.

Metabolite profiles across 96-hour simulations revealed dynamic compartment-specific signatures that shifted predictably with feeding-fasting cycles (**Figure 2B**). At the beginning of the feeding period, metabolite profiles clustered tightly within their respective compartments, reflecting the compartment-specific metabolic activity following fasting, with

246 overlapping cecum and colon profiles, consistent with their similar environments and
247 functionality. Notably, the unprocessed diet formed a distinct cluster, that remained separated
248 from all gut compartments throughout simulations**,** demonstrating that microbial communities
249 extensively transform dietary inputs into modified metabolite profiles rather than simply
250 passing through dietary compounds unchanged. As feeding progressed, jejunal and ileal
251 profiles showed increased dispersion, with the ileum shifting away from the cecum and colon
252 and aligning more with the duodenum and jejunum, likely reflecting intensified nutrient
253 processing as digesta transit accelerates. Cecal and colonic profiles remained stable and
254 distinct, reinforcing their role as fermentation sites. During fasting, distal compartments
255 maintained their clustering but shifted modestly toward the small intestine, while jejunal and
256 ileal profiles converged, consistent with retrograde flow (reflux) of contents during periods of
257 reduced peristaltic activity and nutrient scarcity, which redistributes metabolites backward
258 along the GIT. The reflux mechanism is likewise responsible for the observed similarity in
259 profiles between the duodenum and the gizzard.
260
261 Analysis of specific metabolite classes further illustrated these compartmental and temporal
262 dynamics (**Figure 2C,D**). Simple sugars such as glucose, fructose, and sucrose accumulated in
263 the duodenum and jejunum during feeding periods but were largely depleted in distal
264 compartments. Residual glucose observed in the cecum and colon originated from the
265 progressive breakdown of starch-derived oligosaccharides (maltoundecaose, maltohexaose,
266 amylotriose). During fasting, glucose levels increased in the small intestine as a consequence
267 of reflux and continued digestion of residual oligosaccharides. During the feeding period,
268 amino acids including methionine, threonine, and alanine peaked in the duodenum and jejunum
269 and declined downstream, reflecting rapid absorption in the small intestine; during fasting,
270 reflux redistributed amino acids in upstream compartments, sustaining microbial growth in the
271 absence of dietary inputs. Fermentation products (acetate, propionate, butyrate, ethanol, lactate
272 and formate) reached the highest concentrations in the cecum and colon, particularly during
273 fasting when the community relies on residual substrates from starch digestion and dietary fiber
274 components.
275
276 Beyond accurately recapitulating concentration changes in primary substrates and fermentation
277 products, the model also captured expected spatial and temporal dynamics of bile acids, fatty
278 acids, and neuroactive metabolites. For example, concentrations of the secondary bile acid
279 glycochenodeoxycholate peaked in the duodenum and jejunum during feeding and sharply

280 declined in downstream compartments, while fasting caused modest increases in the upper
281 compartments due to reflux (**Figure 2C**). Hexanoate concentrations peaked in the upper GIT
282 (gizzard, duodenum, jejunum) during fasting, likely due to reflux-mediated redistribution,
283 consistent with previous reports of higher medium-chain fatty acids in the chicken upper GIT
284 relative to the lower GIT[40]. Interestingly, gamma-aminobutyric acid (GABA), a
285 neurotransmitter produced by the gut microbiota and known for its neuroactive roles[41], showed
286 distinct temporal shifts across the GIT (**Figure 2C**). After fasting, GABA concentrations were
287 highest in the cecum and colon (0.0025 ± 0.0007 and 0.0023 ± 0.0005 mM, respectively),
288 reflecting sustained microbial production overnight. During feeding, concentrations increased
289 in the duodenum (22-fold, to 0.0016 ± 0.0007 mM) and ileum (to 0.0023 ± 0.0011 mM). The
290 jejunum showed the greatest fluctuation of GABA across the feeding-fasting cycle (Δ0.0025
291 mM), while cecal and colonic concentrations remained relatively stable. Such findings may
292 have implications for the dynamics of GABA availability and its role in the gut-brain axis.
293
294 The time-dependent changes in metabolite concentrations observed *in silico* reveal how gut
295 microbial communities respond to substrate availability and gut motility. Additionally, these
296 temporal patterns highlight a critical methodological consideration: metabolite concentrations
297 vary dramatically with sampling time. For instance, during fasting, SCFA levels peak in the
298 cecum and colon, as fermentation intensifies and transit slows, allowing accumulation. Such
299 findings underscore the importance of the timing of sample collection in experimental studies
300 of gut metabolism[42].

301 Supplementation with L-threonine or starch is predicted to enhance SCFA 302 production by diverse microbial communities

303 Establishing a model that recapitulates the spatial dynamics of metabolism in the chicken GIT,
304 provides a valuable framework for examining the impact of dietary supplements. Of particular
305 interest is understanding how differences in gut microbial communities may impact results and
306 which supplements may be least susceptible to variations in these communities. With
307 established roles in gut health[11], we focused investigations on the production of SCFAs and
308 screened 34 candidate supplements including established prebiotics (e.g., inulin[112], XOS[113],
309 GOS[114] and MOS[115]), non-digestible carbohydrates with documented beneficial effects on
310 chicken gut health and performance (e.g., beta-glucans[116], arabinooligosaccharides[117], resistant
311 starches[118,119]), essential nutrients commonly supplemented in poultry feed (e.g., thiamin[119],
312 riboflavin[120] and zinc[121]), and metabolites identified through flux balance analysis as potential

growth-limiting factors for beneficial bacteria (e.g., raffinose, L-leucine and pantothenic acid). Simulations involving supplementation of each metabolite were performed for 96-hours for each of the ten communities sampled (5 wheat-based and 5 corn-based with 5 technical *in silico* replicates performed for each community, see Methods).

Overall, we found that the metabolic response of each supplement varied according to both the supplement itself and the type of community (i.e., wheat- vs corn-based; **Figure 3A; Figure S4**). Further analysis of SCFA production fluxes demonstrated that multiple supplements could substantially alter SCFA production rates (**Figure 3B,C; Figure S4**). For instance, high doses of amino acid supplementation showed consistent results: L-threonine and glycine were predicted to significantly increase acetate production in both ileum and cecum irrespective of baseline community composition. Selected complex carbohydrates demonstrated similarly robust impacts: high doses of starch and cellulose were predicted to enhance production of all three SCFAs in both the ileum and cecum relative to controls. Several compounds displayed dose-dependent effects, with opposing outcomes at different concentrations (**Figure S4**). Most notably for propionate production: maltoheptaose supplementation at lower doses had minimal impact, while higher doses significantly decreased production, particularly in the cecum. Pantothenic acid showed similar concentration-dependent divergence, with low doses predicted to enhance SCFA production while higher doses reduced production. These opposing responses likely reflect shifts in community dynamics where higher substrate concentrations may favor fast-growing species that outcompete SCFA producers, reducing community-level yields. Conversely, certain commonly used additives in poultry production (e.g., riboflavin[43], several mannooligosaccharides[44,45]) were unexpectedly predicted to decrease SCFA production across samples. Polysaccharide chain length also influenced SCFA production, with longer lengths of starch and mannooligosaccharides decreasing SCFA production. This is likely a consequence of longer chains requiring more specialized or complete sets of degradation enzymes, which are encoded by fewer bacterial genomes in the community.

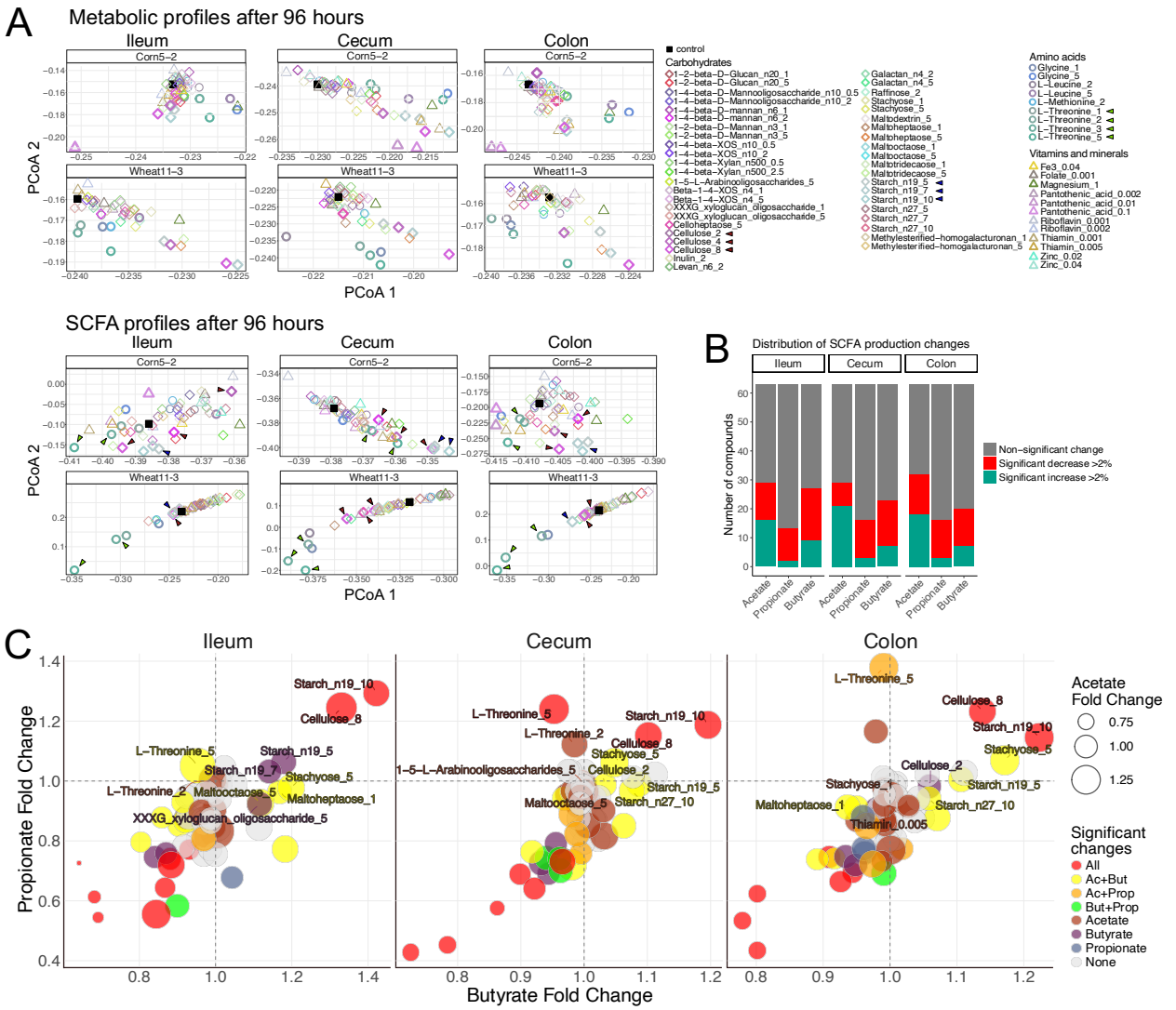

Figure 3. **Impact of dietary supplementation on metabolite profiles and SCFA production across gut compartments. A.** PCoA of metabolite concentrations after 96-hour simulations. Representative samples from corn-fed (Corn5-2) and wheat-fed (Wheat11-3) chickens are shown, comparing control conditions (black dots) with various dietary supplements across the ileum, cecum, and colon compartments. Key compounds discussed in the Results section (L-threonine, starch, pantothenic acid, cellulose, high-dose amino acids) are emphasized with thicker outlines. Arrows indicate L-threonine, cellulose, and starch - the three compounds selected for validation trials. Top panels: PCoA based on all metabolite concentrations. Bottom panels: PCoA based solely on SCFA concentrations. Supplement types are indicated by symbols and colors, with dosing shown after underscores (e.g., Inulin_2 = 2g per 100g diet). Complete dataset including all samples and compartments is presented in Supplementary Figure 4. **B.** Distribution of SCFA production responses to supplementation. Stacked bar plots show the proportion of tested compounds that significantly increased (green), decreased (red), or did not affect (gray) community-level SCFA production in each compartment. **C.** Scatter plots showing fold changes in butyrate (x-axis) versus propionate (y-axis) production for all tested supplements. Bubble size represents the magnitude of acetate fold change. Colors indicate which SCFA changes were statistically significant: red = all three SCFAs; yellow = acetate + butyrate; orange = acetate + propionate; green = butyrate + propionate; brown = acetate only; purple = butyrate only; blue-gray = propionate only; transparent gray = no significant changes. Dashed lines at fold change = 1.0 indicate average production levels in control simulations.

361 To identify promising candidates for potential application in the poultry industry, we focused
362 on supplements that consistently increased SCFA production. Across compartments and diets,
363 three supplements, namely, cellulose, starch, and L-threonine, were predicted to consistently
364 enhance SCFA production (**Figures 3A,C; Figure S4B**). Cellulose, a complex polysaccharide,
365 serves as a dietary fiber in poultry nutrition[46,47] and is primarily fermented to produce SCFAs
366 by cellulolytic bacteria such as Ruminococcaceae, Lachnospiraceae, and other Clostridiales[48].
367 Starch, a readily fermentable carbohydrate, is a major energy source for both the host and its
368 gut microbiota. The digestion of starch starts in the small intestine, and a portion reaches the
369 lower GIT, where bacterial enzymes degrade it into fermentable oligosaccharides and
370 monosaccharides, subsequently converted to SCFAs through microbial fermentation pathways.
371 L-threonine is an essential amino acid for chickens[124]. While primarily absorbed in the small
372 intestine, a fraction of dietary L-threonine can reach the cecum and colon, where it serves as a
373 substrate for bacterial species encoding threonine degradation pathways, yielding acetate and
374 propionate as byproducts[49–51]. Based on their reproducible *in silico* effects across diverse
375 microbial communities within the reference dataset, we selected these three candidates for
376 validation in chicken feeding trials, testing two dietary doses of each to determine whether
377 predicted metabolic benefits translated *in vivo*.

378 Context-specific community models improved prediction accuracy

379 To evaluate the predictive capacity of our modeling framework, we performed a trial
380 investigating the impact of two doses each of cellulose, starch, and L-threonine
381 supplementation in broilers fed a corn-based diet. Ileal and cecal samples were collected at day
382 14 for 16S rRNA sequencing and targeted metabolomics (see Methods). Comparisons between
383 predicted and experimentally derived metabolite concentrations revealed a spectrum of
384 correlations (**Figure 4A**, upper panel). Among the metabolites tested, butyrate and fumarate
385 concentration fold changes showed the highest agreement between predictions and
386 experimental measurements (Spearman's ρ=0.49 for both; **Figure 4B**). In contrast, acetate
387 (Spearman's ρ=-0.14), succinate (Spearman's ρ=0.09), and α-ketoglutarate (Spearman's ρ=-
388 0.2) did not correlate with predictions, while lactate predictions were inversely correlated with
389 trial measurements (Spearman's ρ=-1.0, q=0.039). A potential confounder in these correlations
390 is the microbial community composition, which differed between the validation trial
391 (conducted in Guelph, Ontario) and the original trial used to construct the six-compartment
392 models (conducted in Edmonton, Alberta). PCoA of cecal 16S rRNA profiles revealed distinct
393 clustering of the trial-derived communities compared to both the original full-resolution dataset

394 and the simplified composition used in the 6-compartment model (**Figure 4B**). PERMANOVA
395 analysis confirmed statistically significant differences in community composition ($p < 0.05$)
396 across both treatment groups and data sources, indicating substantial shifts in community
397 structure between cohorts.
398
399 These compositional differences reflected distinct taxonomic distributions between trials
400 (**Figures S1, S6**). For example, Lactobacillaceae were more abundant in the original reference
401 dataset (average 5.3 ± 3.9%, **Figure S1**) compared to trial communities (average 0.51 ± 1.88%,
402 **Figure S6**) in cecal samples, contributing to predicted lactate accumulation in the original
403 model and likely explaining the negative correlation for lactate. Notably, Enterobacteriaceae
404 dominated the cecum in the reference dataset (average 21.3 ± 7.8%) but were nearly absent in
405 trial communities (average 0.85 ± 1.8%). As facultative anaerobes, Enterobacteriaceae, mainly
406 represented by *E. coli* in our models, produce acetate, succinate, and formate as major end
407 products (**Figure 2A;Figure S8**) and are known to mediate cross-feeding networks in cecal
408 communities[20]. The combined depletion of these families could alter both metabolite
409 production and metabolic interactions, potentially explaining poor predictions for acetate and
410 succinate. Conversely, Ruminococcaceae expanded from 4.2 ± 3.0% (reference) to 29.4 ± 8.4%
411 (trial) in the cecal communities. This family comprises obligate anaerobic fiber degraders
412 known to produce butyrate, including *Faecalibacterium*, a key butyrate producer in our models
413 (**Figure 2A;Figure S8**). This may explain why butyrate predictions maintained reasonable
414 correlation (Spearman's ρ=0.49) despite the community restructuring. These findings
415 demonstrated that while metabolic predictions were robust to variation within a reference
416 cohort (**Figure 3**), community composition differences between facilities impacted prediction
417 accuracy for certain metabolites, highlighting the need for context-specific modeling.

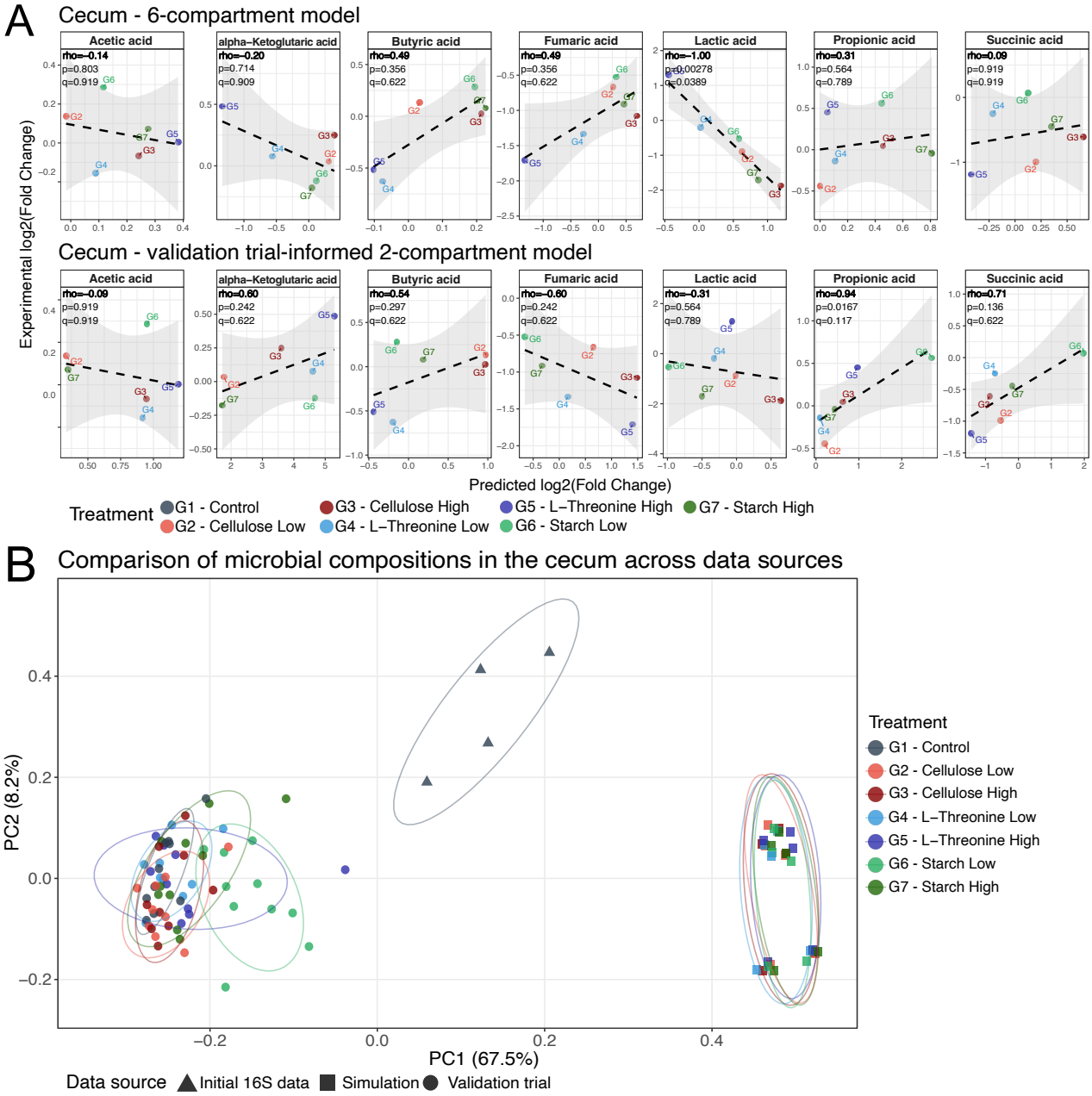

Figure 4. Trial-specific community composition data substantially improves metabolic predictions for cecal fermentation. A. Correlation between predicted and experimental $\log_2$(fold change) values for seven fermentation metabolites in the cecum. Top row: Predictions from the 6-compartment model after 96-hour simulations compared to experimental measurements from the validation trial. Bottom row: Predictions from the trial-informed 2-compartment model after 48-hour simulations compared to experimental measurements. Each panel shows one metabolite with treatment groups indicated by color. Dashed lines represent linear regression fits. Spearman correlation coefficient (rho), uncorrected p-value (p), and FDR-adjusted q-value (q) are displayed for each metabolite. Fold changes were calculated relative to control group medians. **B**. Community composition differences. PCoA plots comparing taxonomic profiles between original reference data (Initial data), simplified model communities (Simulation), and trial communities (Validation trial) for cecum. PERMANOVA confirms significant separation between data sources ($p < 0.05$), highlighting taxonomic basis for model refinement.

433 To address this limitation, we constructed a two-compartment model (reflecting the two
434 compartments sampled in the validation trial – ileum and cecum) based on communities from
435 the trial 16S profiles (see Methods). Trial-informed models were found to increase prediction
436 accuracy across multiple metabolites (**Figure 4A**, lower panels). For instance, propionate
437 correlation increased substantially from Spearman's ρ=0.31 to ρ=0.94 (**Figure 4A**), aligning
438 with elevated concentrations in the low-starch treatment group where *Bacteroides* were
439 uniquely detected (**Figure S6)**. Similarly, predictions for succinate improved from Spearman's
440 ρ=0.09 to ρ=0.71, and α-ketoglutarate from Spearman's ρ=-0.2 to ρ=0.6. Butyrate correlation
441 showed modest improvement (Spearman's ρ=0.49 to ρ=0.54), while lactate predictions shifted
442 from significant inverse correlation (Spearman's ρ=-1.0, q=0.03) to a more moderate mismatch
443 (Spearman's ρ=-0.31), consistent with reduced Lactobacillaceae abundance in trial-derived
444 inputs. However, even with trial-specific community data, the models failed to accurately
445 predict certain metabolites, revealing limitations beyond community composition effects.
446 Acetate, which is broadly produced and absorbed throughout the gut, remained poorly
447 predicted (Spearman's ρ=-0.14 to ρ=-0.09), a pattern consistent with acetate prediction
448 challenges reported in previous community modeling studies[52]. Fumarate correlation declined
449 (Spearman's ρ=0.49 to ρ=-0.60), with measured concentrations showing consistent depletion
450 across all dietary treatments (ileum Kruskal-Wallis (KW) p=0.004, cecum KW p=0.002,
451 significant post-hoc Dunn and Wilcoxon rank-sum tests, **Figure S7AB**), despite predicted net
452 microbial production suggesting rapid microbial consumption or host absorption not captured
453 in the model. In contrast, butyrate increases under low-dose cellulose and starch
454 supplementation aligned well with predicted production by members of Ruminococcaceae,
455 Butyricicoccaceae, and Lachnospiraceae families (cecum KW p=0.029), demonstrating
456 accurate predictions when key producer taxa were present (**Figure S8**).
457
458 We note that high inter-individual variability and small sample sizes (n=6 per treatment)
459 limited detection of statistically significant patterns for several metabolites, though trial-
460 informed models consistently improved rank-order agreement with experimental trends.
461 Together, these results demonstrate that community-matched metabolic models can reproduce
462 *in vivo* fermentation patterns when grounded in appropriate taxonomic inputs, though host
463 metabolic processes and biological variability remain important sources of prediction
464 uncertainty.
465

DISCUSSION

Optimizing poultry nutrition to promote gut health requires an understanding of how dietary inputs are transformed into metabolic outputs across the gastrointestinal tract. We developed a spatiotemporally resolved computational framework that simulates microbial community metabolism throughout the chicken GIT. This framework represents the most comprehensive spatial characterizations of gut metabolism in any livestock system performed to date. Our multi-compartment model captures three critical features: 1) spatial organization across the entire GIT through the simulation of six connected compartments; 2) temporal dynamics through inclusion of feeding-fasting cycles; and 3) the bidirectional flow of microbes and metabolites between neighbouring compartments through peristalsis and reverse peristalsis. Together these features represent a significant advance over previous metabolic modeling efforts in poultry that focused specifically on cecal metabolism[19,20]. By incorporating five additional compartments (gizzard, duodenum, jejunum, ileum, and colon), our framework treats the cecum as part of an interconnected system where upstream metabolic interconversions reshape substrate availability in the lower GIT and downstream metabolism. Our simulations revealed that metabolite landscapes and production rates vary substantially across compartments and over time – patterns that single-compartment models cannot capture. Upper gut compartments displayed distinct metabolic profiles enriched for bile salt hydrolases, membrane lipid synthesis, and fatty acid biosynthesis, while cecal and colonic communities specialized in SCFA synthesis pathways and polysaccharide degradation. The unprocessed diet remained distinct from metabolic profiles of all gut compartments throughout simulations, demonstrating that microbial communities extensively transform dietary inputs rather than simply passing compounds unchanged. Importantly, overnight reflux redistributes metabolites and helps explain convergences in metabolite profiles between adjacent regions.

Recent advances in mammalian gut modeling, including multi-compartment frameworks in mice[13,53], human community-level FBA approaches[8,12,54], and the CODY model of the human colon[16], have demonstrated the value of spatially explicit and physiologically informed models for understanding host-microbiome metabolism. Our work builds on these concepts and extends them to poultry, where avian-specific physiological features, such as rapid upper GIT transit, steep oxygen gradients, and reverse peristalsis, play a defining role in nutrient processing and microbial ecology. Incorporating these traits allowed us to capture metabolite redistribution and temporal oscillations characteristic of the chicken gut. By modeling taxa

individually rather than as a single metabolic entity, we predicted taxon-specific contributions to SCFA production: *Bacteroides* as the primary propionate producers, *Faecalibacterium* and *Clostridium* spp. as key butyrate producers, and Enterobacteriaceae and Lachnospiraceae as major acetate producers. Our study showed that the upper GIT (gizzard, duodenum and jejunum) communities were dominated by facultative anaerobes encoding fewer metabolic enzymes and enriched for bile salt hydrolases and fatty acid biosynthesis, reflecting adaptation to readily available nutrients under aerobic conditions. The ileum harbored mixed aerobic and anaerobic taxa, reflecting its transitional position between upper and lower GIT, while cecal and colonic communities were enriched in Clostridiales families with the capacity to ferment complex polysaccharides. Through the inclusion of spatial and temporal dynamics, our model captured metabolite accumulation associated with fasting and reflux. For example, fasting was associated with an increase in the production of SCFAs in the lower GIT (cecum and colon) as well as signaling molecules such as GABA in the upper GIT. These observations indicate that the timing of sample collection has the potential to substantially influence metabolite levels, consistent with recent studies showing that feeding cycles drive dramatic differences in metabolic measurements[42].

Having established a spatiotemporally resolved framework, we leveraged its predictive capabilities to systematically screen dietary interventions. Simulations involving 34 candidate metabolite supplements revealed that their impacts were largely context-dependent, with metabolic responses varying by substrate type, concentration, polymer chain length, microbial community composition, and gut compartment. Some additives commonly used in poultry production (riboflavin, mannooligosaccharides) were unexpectedly predicted to decrease SCFA production, while others showed opposite dose-dependent effects (e.g., maltoheptaose, pantothenic acid). However, our model predicted three compounds – cellulose, starch, and L-threonine – to consistently enhance SCFA production across diets and compartments. The robustness of these predicted effects despite high inter-individual microbiome variation were tested in a poultry feed trial, enabling direct assessment of our model's prediction accuracy.

Our experimental validation through a controlled feeding trial yielded critical insights into the determinants of predictive accuracy in community metabolic modeling. Butyrate responses to cellulose and starch supplementation aligned with model predictions, while other metabolites showed variable agreement with experimental measurements. For example, lactate accumulated in simulations but not *in vivo*, which reflected the much lower abundance of

533 Lactobacillaceae in the trial cohort compared to the reference community used for model
534 construction. Similarly, Enterobacteriaceae abundances were substantially lower in trial birds,
535 while Ruminococcaceae increased 7-fold relative to the reference dataset, which could disrupt
536 prediction for metabolites predominantly produced by specific taxa belonging to these families
537 (e.g., acetate, butyrate). Since one of our main aims was to identify supplements that led to
538 robust changes in SCFA production irrespective of community composition, this finding
539 suggests that predictions may have limited relevance for poultry raised under different
540 conditions and/or locales. By incorporating 16S rDNA survey data collected from the ileum
541 and ceca during the trial within a more simplified two-compartment model, prediction accuracy
542 improved, particularly for propionate, succinate, and α-ketoglutarate (Spearman's
543 ρ=0.31→0.94; ρ=0.09→0.71; and ρ=-0.20→0.60, respectively). This improvement
544 underscores taxonomic structure as a primary determinant of metabolic function, aligning with
545 recent observations that community composition drives differences in SCFA production[12]. At
546 the same time, we note that even trial-informed model could not predict acetate (Spearman's
547 ρ=-0.09), consistent with challenges reported in other community modeling studies, or
548 fumarate (Spearman's ρ=-0.60), which showed consistent experimental depletion despite
549 predicted microbial production, likely reflecting rapid host absorption not captured by our
550 simplified fractional removal rates. This suggests future models could be improved through an
551 improved understanding of host-metabolite absorption. These findings highlight that while
552 metabolic predictions were robust to dietary and inter-individual variation within a reference
553 cohort, cross-facility differences in community composition significantly impact accuracy, and
554 host metabolic processes remain important sources of uncertainty.
555
556 Implementation-specific limitations are more readily addressable as data availability improves.
557 The model's reliance on automated genome-scale reconstructions means that enzymatic
558 capabilities may be incomplete for underrepresented taxa. Our framework currently models
559 only bacteria, excluding fungi and other microorganisms that may contribute to gut
560 metabolism. The model assumes uniform distribution and mixing within the compartments,
561 which may not accurately reflect the spatial microenvironments where localized metabolite
562 gradients shape community interactions. Estimated rates of nutrient absorption and gut transit
563 show inter-individual variation that our population-averaged parameters cannot capture.
564 Additionally, the absence of host metabolic networks means we cannot represent how host
565 processes (e.g., immune responses) affect microbial metabolism. Nevertheless, this modeling
566 framework is adaptable and can readily accommodate future advances in microbial genomics

567 and metabolic modeling. As new high-quality poultry MAGs and physiological measurements
568 become available, they can be readily incorporated in future models. Incorporating gene and
569 protein expression (metatranscriptomic and proteomic data) will further improve the accuracy
570 of individual reconstructions, while coupling microbial models with host metabolic networks
571 would improve representation of host absorption and host-microbiome metabolic exchange.
572
573 While our six-compartment model represents a significant step forward, it serves as a proof-
574 of-concept for systematic modeling of the poultry GIT. By bridging *in silico* predictions with
575 controlled feeding trials, we demonstrate both the promise and the limitations of current
576 metabolic modeling approaches. This work lays the foundation for evaluating dietary
577 interventions in poultry, guiding the design of targeted supplements that enhance SCFA
578 production and gut health. More broadly, it illustrates how multi-compartment community
579 models can accelerate hypothesis generation, reduce reliance on large-scale animal trials, and
580 extend to other host-associated microbiomes where spatial structure and host physiology play
581 decisive roles.
582

583 # METHODS

584 ## Development of a six-compartment spatiotemporal model

585 ### Processing of 16S rRNA gene data

586 Reads were processed using the QIIME2[55] package (version 2023.2), which involved trimming,
587 filtering, and removing low-quality and chimeric sequences. The resulting high-quality data
588 was then processed following the deblur pipeline. Sequences were clustered into amplicon
589 sequence variant (ASV) groups and singleton sequences removed. Taxonomic classification
590 was performed using the classify-hybrid-vsearch-sklearn function against the SILVA database
591 (release 138.1)[55,56]. ASVs with an abundance less than 0.01% were removed to reduce the
592 potential for observing bleed-through ASVs. ASVs identified as chloroplast or mitochondrial
593 contaminants were also removed, and ASV tables were subsequently normalized and rarefied
594 to a depth of 10,000 reads per sample to ensure comparability across datasets.

595 ### Selection of representative species and model reconstruction

596 To represent the most abundant taxa within each gut compartment, the top five ASVs per
597 bacterial family were used as blastn queries against several collections of high-quality chicken
598 gut-derived MAGs: a set of 12,339 MAGs from integrated 799 public chicken gut microbiome

599 samples[28], 469 MAGs from 24 chicken cecum samples[27], and 461 MAG from five chicken gut
600 compartments of 30 chickens[29]. Sequences meeting thresholds of 97% identity, e-value
601 threshold of 1e-70, as well as passing assembly quality thresholds of ≥90% completeness, and
602 ≤5% contamination were retained for further analysis. For ASVs that did not yield any MAG
603 matches meeting these criteria, the 16S rRNA sequence was subjected to a blastn search against
604 the NCBI RefSeq 16S database[57]. The highest scoring sequence alignments were then
605 evaluated based on three criteria: (i) presence in chicken gut-derived MAG collections, (ii)
606 prior documentation in poultry microbiome studies, and (iii) transcriptional activity confirmed
607 by metatranscriptomic data from the same reference trial[5]. MAGs for taxa meeting these
608 criteria and representing the most prevalent members of their genus in the chicken gut were
609 selected for downstream metabolic model reconstruction. Complete details of genome sources,
610 genome quality metrics, and taxonomic classifications for all selected MAGs are provided in
611 Supplementary **Table S1**. Gapseq version 1.2[30] with default settings was used to reconstruct
612 genome-scale metabolic models. Draft metabolic models were curated manually to improve
613 representation of carbohydrate metabolism (see Supplementary Methods).

614 **Construction of sample-specific gut microbiota community models**

615 Compartment-specific models were constructed for 60 samples (2 diets × 5 birds × 6
616 compartments) using the list of mapped taxa and their family-level abundances from 16S data.
617 Representative species models were combined according to compartment-specific abundance
618 profiles. In cases where sequencing data were unavailable for one compartment within a
619 sample, the missing values were imputed using average relative abundances from the same
620 dietary group and compartment. Samples missing data for more than one compartment were
621 excluded.

622 **Simulation framework and gastrointestinal configuration**

623 All microbial community simulations were conducted using BacArena, an R-based platform
624 for community modeling[9]. Bacteria were represented as individual agents occupying a 100 ×
625 100 grid (10,000 cells total), where each cell could grow, move, and exchange metabolites with
626 the surrounding environment. Growth optimization was performed for each individual at every
627 time step using the microbial biomass reaction as an objective. Simulations were run for 96
628 hours (six-compartment model) or 48 hours (two-compartment model), each consisting of a
629 16-hour daytime phase (representing daylight exposure and feeding) followed by an eight-hour
630 nighttime phase (mimicking sleeping and fasting conditions). To account for stochasticity in
631 bacterial placement, movement, and replication, each bird-specific model was simulated with

632 5 replicates using different random seeds. The simulations were conducted with a time step of
633 1 hour, representing an hour of bacterial growth per iteration. To incorporate physiological
634 factors, including absorption, peristalsis, reflux (reverse peristalsis), feeding, excretion, pH and
635 oxygen homeostasis, the simulation environment was updated every hour (see more details in
636 the **Supplementary Methods**). After each hour of simulation, these processes were executed
637 to adjust the environment accordingly before proceeding with the simulation. The relevant
638 parameters used during simulation initialization were defined for each compartment based on
639 literature sources (**Table S2A).**

640 **Comparative analysis of the functional capabilities of community models**

641 To compare the metabolic capabilities across different gut compartments and samples, I first
642 extracted the complete set of reactions from their respective community metabolic models. To
643 quantify the metabolic potential within each sample, accounting for the varying contributions
644 of different species, I summarized the reaction counts within each sample, where each reaction
645 count was weighted by the relative abundance of the species contributing to that reaction. The
646 resulting incidence matrices contained information on the reaction abundance in each
647 community. Bray-Curtis dissimilarity matrices were constructed from the incidence matrices
648 described using *vegdist* function from the vegan R-package, and Principal Coordinate Analysis
649 was performed using *cmdscale* function from stats R-package.

650 **Comparison of control simulations and simulations with supplementation**

651 To evaluate the effects of different compounds on community fluxes and metabolite
652 concentrations, fold changes were calculated for each combination of gut compartment,
653 metabolite, and supplemented compound by dividing the metabolite concentration or
654 community flux in the experimental group by the mean concentration or flux of 5 replicates
655 from the control group. Additionally, given the experimental design, where validation is
656 performed through chicken trials using 10 chickens per treatment, I subsampled 10 replicates
657 from the original 25 by randomly selecting 2 out of 5 replicates from each of the 5 samples per
658 diet. This subsampling approach resulting in 10 subsampled replicates per condition was
659 designed to match the number of biological replicates to be used in the experimental validation
660 and maintain the integrity of the statistical comparisons. Significant differences were
661 determined by Wilcoxon signed-rank tests, that were conducted on the fold changes under the
662 null hypothesis that the median fold change is equal to 1 (indicating no effect of the treatment).
663 P-values were calculated using a two-sided test, and to account for the multiple comparisons
664 inherent in this analysis, the Benjamini-Hochberg procedure was applied to control the False

665 Discovery Rate (FDR). Results were considered statistically significant at an FDR-adjusted p-
666 value threshold of 0.05.

667 Experimental validation and trial-informed model refinement

668 *In vivo* validation through chicken trials

669 While *in silico* simulations demonstrated significant effects of supplementation over 96 hours,
670 the translation between *in silico* time units and actual community dynamics *in vivo* is not direct.
671 Microbial growth rates, metabolic activities, and community interactions in the living gut are
672 influenced by multiple physiological factors not fully captured in the model. Therefore, to
673 ensure sufficient time for supplement-induced changes to manifest in the gut microbiome, a
674 longer supplementation period was implemented in the validation experiments.
675 Seventy one-day-old broiler chickens were raised on standard corn-based starter diet for 7 days
676 before random assignment to seven treatment groups (n=10 per group): control (G1), cellulose
677 at 2g/100g (G2) and 8g/100g (G3), L-threonine at 1g/100g (G4) and 5g/100g (G5), and starch
678 at 5g/100g (G6) and 10g/100g (G7). Supplementation lasted 7 days, birds were euthanized on
679 day 14 and samples were collected from ileum and cecum, stored on dry ice, and then kept at
680 −80 °C for microbiome analysis. All animal experiments were approved by the Animal Care
681 Committee of the University of Guelph and adhered to the guidelines for the use of animals
682 (Animal Utilization Protocol #4815).
683

684 DNA extraction

685 DNA was extracted from 10 mg of chicken gut samples (ceca and ileum) using the
686 ZymoBIOMICS DNA miniprep kit with the addition of the ZR BashingBead (2.0 mm) tubes
687 to increase homogenization and lysis of the samples. The extraction protocol was followed as
688 indicated in the manual with a final elution volume of 50uL. 5 µL of the ZymoBIOMICS Spike-
689 In Control I (D6320) was added to ileum samples and 10 µL to caeca. Positive (Zymo Microbial
690 Community Standard) and negative (no input) extraction controls were run alongside the
691 sample extractions.

692 16S rRNA gene sequencing and processing

693 The V4 hypervariable region of the 16S rRNA gene was amplified using uniquely barcoded
694 515F (forward) and 806R (reverse) sequencing primers to allow for multiplexing[58].
695 Amplification reactions were performed using 12.5 µL of KAPA2G Robust HotStart
696 ReadyMix (KAPA Biosystems), 1.5 µL of 10 µM forward and reverse primers, 7.5 µL of sterile

697 water and 2 µL of DNA. The V4 region was amplified by cycling the reaction at 95°C for 3
698 minutes, 18x cycles of 95°C for 15 seconds, 50°C for 15 seconds and 72°C for 15 seconds,
699 followed by a 5-minute 72°C extension. All amplification reactions were done in duplicate to
700 reduce amplification bias, pooled, and checked on a 1% agarose TBE gel. Pooled duplicates
701 were quantified using PicoGreen and combined by even concentrations. The library was then
702 purified using Ampure XP beads and loaded on to the Illumina MiSeq for sequencing,
703 according to manufacturer instructions (Illumina, San Diego, CA). Sequencing is performed
704 using the V2 (150bp x 2) chemistry. A single-species (*Pseudomonas aeruginosa* DNA), a mock
705 community (Zymo Microbial Community DNA Standard) and a template-free negative control
706 were included in the sequencing runs. Sequencing data were processed using the identical
707 QIIME2 pipeline detailed in section "Processing of 16S rRNA gene data" above, ensuring
708 direct comparability between reference and trial datasets.

709 **Targeted quantitative metabolomics data processing and analysis**

710 A targeted quantitative metabolomics workflow was performed using a custom reverse-phase
711 LC-MS/MS assay on an AB Sciex 5500 QTRAP® (Applied Biosystems/MDS Sciex) equipped
712 with an Agilent 1290 UHPLC. Metabolites were identified and quantified by multiple reaction
713 monitoring using isotope-labeled and other internal standards. The assay was prepared in a 96-
714 deep-well plate format with an attached filter plate; the first 14 wells were allocated to one
715 blank, three zero samples, seven calibration standards, and three quality control samples.
716 For all metabolites except organic acids, samples were thawed on ice and extracted. Extracts
717 were loaded onto the filter plate, dried under nitrogen, derivatized with phenyl-isothiocyanate,
718 incubated, and dried again. Metabolites were then extracted with 300 µL extraction solvent and
719 collected by centrifugation into the lower deep-well plate, followed by dilution with MS
720 running solvent. For organic acids, 150 µL ice-cold methanol and 10 µL isotope-labeled
721 internal standard mix were added to extracted samples for overnight protein precipitation.
722 Samples were centrifuged at 13,000×g for 20 min, and 50 µL supernatant was loaded into a
723 96-deep-well plate. 3-nitrophenylhydrazine reagent was added, followed by 2h incubation;
724 BHT stabilizer and water were then added prior to LC-MS injection. Samples were analyzed
725 by an LC method followed by a direct injection method. Data were acquired and processed in
726 Analyst v1.6.3.
727 Dry-weight normalized concentrations were processed using MetaboAnalyst web platform[59].
728 Quality control filtering removed low-variance features (interquartile range < 5th percentile)
729 and low-abundance features (median intensity < 5th percentile). The filtered dataset was

normalized using probabilistic quotient normalization (PQN) with the control group (G1) as reference to account for dilution effects and technical variation. Fold changes for each metabolite were calculated relative to the control group median within each compartment. Statistical comparisons between treatment and control groups employed two-sample Wilcoxon tests with Benjamini-Hochberg FDR correction. To evaluate agreement between model predictions and experimental results, Spearman's rank correlation coefficients were computed across all metabolites and treatment conditions, comparing predicted and observed fold changes within each compartment.

Construction of trial-informed 2-compartment models

From 16S rRNA data of 112 samples, 694 ASVs were filtered to retain those with ≥0.5% relative abundance, reducing sequencing noise. Functional profiles were predicted using PICRUSt2[60], and ASVs were clustered by enzymatic similarity (Jaccard distance, 0.85 threshold), yielding 267 functionally distinct representatives. These were matched to high-quality MAGs through blastn-search against four chicken MAG catalogues: 461 MAG from five chicken gut compartments of 30 chickens[29], MGnify chicken-gut v1.0 collection (13,386 genomes)[61], a set of 12,339 MAGs from integrated 799 public chicken gut microbiome samples[28], and 461 MAG from five chicken gut compartments of 30 chickens[29]. Matching was performed in three sequential passes on unmatched ASVs: (i) 97% sequence identity threshold with ≥80% query coverage; (ii) 95% identity with ≥70% coverage; (iii) 90% identity with ≥70% coverage. For each BLAST hit, a combined quality score was computed incorporating both sequence similarity (60% weight) and assembly quality (40% weight), where: sequence similarity = 0.4*identity + 0.3*coverage + 0.3*min[100,100×bitscore/500]), assembly quality = completeness - 5*contamination. Final selection included top-scoring hits per ASV, resulting in 170 unique MAGs. Complete details of genome sources, genome quality metrics, and taxonomic classifications for all selected MAGs are provided in Supplementary **Table S3**. Metabolic models were reconstructed using gapseq version 1.4.0[30] with default settings for 44 bird pairs with sufficient data quality.

Bird-specific models paired ileal and cecal communities based on sample-derived ASV abundances, creating 88 compartment-specific models (44 birds × 2 compartments). Model assembly followed the same procedure as for the multi-compartment system, ensuring direct comparability.

761 **Definition of *in silico* dietary input**

762 Nutritional information from the corn-based grower diet was adjusted to account for upstream
763 digestion and absorption to create an *in silico* representation of dietary metabolites reaching
764 the distal small intestine. The base diet composition was derived from the same poultry feed
765 tables used in the 6-compartment model, with modifications to simulate the metabolic
766 environment of the distal jejunum/proximal ileum. Metabolite concentrations entering the
767 ileum were reduced based on published ileal digestibility coefficients for corn-based poultry
768 diets. Mineral retention rates were set according to jejunal and ileal digestibility studies[62–68].
769 Similarly, carbohydrate retention reflected measurements on upper small intestine digestion[69–
770 71], while amino acids were retained at 25% based on typical ileal digestibility[69,72]. Fatty acid
771 retention varied by saturation level[73], and cellulose was retained at 50% to reflect partial
772 fermentation in the upper gut. Essential metabolites (host-supplied metabolites, such as mucins,
773 urea, and metabolites supporting growth of all community members) were added at baseline
774 concentrations. The composition of the *in silico* diets used is available in the **Table S4**.

775 **Design and simulation of a trial-informed 2-compartment (ileum-cecum) model**

776 The design and configuration were identical to the six-compartment GIT simulation framework
777 (described in the **Supplementary Methods**) with all the processes applicable to ileum and
778 cecum implemented in the same way, except the reflux happening overnight. In the simplified
779 2-compartment model, reverse peristalsis was not considered due to the lack of upstream
780 compartments and colon, involved in the process.

781 To maintain realistic metabolic growth rates, we implemented cooperative trade-off FBA
782 (ctFBA) with L2 regularization, adapted from the MICOM framework[8]. This approach
783 balances individual species growth rates against community-level biomass production through
784 a two-step optimization. First, the maximum total community biomass production rate is
785 determined, then the individual species growth rates are optimized while constraining total
786 community growth to a fraction (τ, trade-off parameter) of the maximum, using L2
787 regularization to minimize growth rate variance. The trade-off parameter (τ) was calibrated
788 independently for each compartment to ensure at least 90% of species achieved positive growth
789 rates while maintaining physiologically realistic maximum growth rates ($<3\ h^{-1}$ in the ileum,
790 $<5\ h^{-1}$ in the cecum). Calibration was performed at simulation initialization using the seeded
791 microbial community and initial medium conditions, similar to MICOM's approach.

792 The relevant parameters used during simulation initialization were defined for each
793 compartment based on literature sources (**Table S2B**).

794 **Simulation of dietary supplementation for validation experiments**

795 To simulate dietary supplementation treatments, supplement concentrations entering the ileum
796 were adjusted to account for upstream absorption and saturation effects. Cellulose
797 supplementation at 2g/100g (G2) and 8g/100g (G3) was modeled as 1g/100g and 4g/100g
798 reaching the ileum, maintaining an approximately 50% passage rate. L-Threonine
799 supplementation at 1g/100g (G4) and 5g/100g (G5) was modeled as 0.4 g/100g and 2.5 g/100g
800 reaching the ileum. While 40-60% of dietary threonine undergoes first-pass gut extraction, high
801 doses saturate intestinal absorption, allowing greater proportions to reach the distal ileum.
802 Starch supplementation at 5g/100g (G6) and 10g/100g (G7) in feed was modeled as 1.25g/100g
803 and 2.0g/100g reaching the ileum, respectively, reflecting saturation of glucose absorption in
804 the proximal small intestine at higher doses. These adjustments ensured physiologically
805 realistic ileal concentrations while maintaining experimental dose-response relationships.
806

DATA AVAILABILITY

For the 6-compartment model, 16S rDNA sequence datasets from a previous trial examining the impact of AGPs and diet on the poultry gut microbiome were downloaded from the SRA (project PRJNA614900). The previous study[5] details the animal trial conditions, sequencing data retrieval, and 16S rDNA sequencing. The 16S rDNA sequence datasets generated in this study from the feeding trial are deposited under the BioProject PRJNA1403483.

CODE AVAILABILITY

Scripts, source data and metabolic models required to reproduce the analyses of this study can be accessed through GitHub at https://github.com/ParkinsonLab/ChickenGIT_modeling

ETHICS DECLARATIONS

COMPETING INTERESTS

The authors declare that they have no competing interests.

FUNDING

This work was funded by grants from the Natural Sciences and Engineering Research Council of Canada to J.P. (RGPIN-2019-06852/RGPIN-2025-06006), and Ontario Research Fund-Research Excellence to J.P. and S.S. High-performance computing was provided by the SciNet HPC Consortium; SciNet is funded by the following: the Canada Foundation for Innovation under the auspices of Digital Alliance Canada, the Government of Ontario, Ontario Research Fund–Research Excellence, and the University of Toronto. The funders had no role in the design of the study, collection of data and analysis, preparation of the manuscript, and decision to publish.

AKNOWLEDGEMENTS

We thank the Centre for the Analysis of Genome Evolution & Function (CAGEF) at the University of Toronto for 16S rRNA amplicon sequencing services and The Metabolomics Innovation Centre (TMIC) for metabolomics profiling services.

AUTHORS' CONTRIBUTIONS

J.P. and I.U. conceived and designed the study. I.U., J.P., M.A. and S.S. designed the validation chicken trials; M.A. and S.S. conducted the chicken feeding trials, obtained regulatory approvals, and collected intestinal samples. I.U. performed metabolic model reconstruction and

curation, simulations, data analyses, and visualization. J.P. and I.U wrote the manuscript. All authors reviewed and/or edited the manuscript.

REFERENCES

1. Dibner, J. J. & Richards, J. D. Antibiotic growth promoters in agriculture: History and mode of action. *Poult. Sci.* **84**, 634–643 (2005).
2. Zhao, C., Wang, Y., Mulchandani, R. & Van Boeckel, T. P. Global surveillance of antimicrobial resistance in food animals using priority drugs maps. *Nat. Commun.* **15**, (2024).
3. Rahman, M. R. T., Fliss, I. & Biron, E. Insights in the Development and Uses of Alternatives to Antibiotic Growth Promoters in Poultry and Swine Production. *Antibiotics* vol. 11 Preprint at https://doi.org/10.3390/antibiotics11060766 (2022).
4. Patience, J. F. & Ramirez, A. Invited review: strategic adoption of antibiotic-free pork production: the importance of a holistic approach. *Translational Animal Science* vol. 6 Preprint at https://doi.org/10.1093/tas/txac063 (2022).
5. Zou, A. *et al.* Systematic profiling of the chicken gut microbiome reveals dietary supplementation with antibiotics alters expression of multiple microbial pathways with minimal impact on community structure. *Microbiome* **10**, (2022).
6. Orth, J. D., Thiele, I. & Palsson, B. Ø. What is flux balance analysis ? *Nat. Biotechnol.* **28**, 245–248 (2010).
7. O'Brien, E. J., Monk, J. M. & Palsson, B. O. Using genome-scale models to predict biological capabilities. *Cell* vol. 161 Preprint at https://doi.org/10.1016/j.cell.2015.05.019 (2015).
8. Diener, C., Gibbons, S. M. & Resendis-Antonio, O. MICOM: Metagenome-Scale Modeling To Infer Metabolic Interactions in the Gut Microbiota. *mSystems* **5**, (2020).
9. Bauer, E., Zimmermann, J., Baldini, F., Thiele, I. & Kaleta, C. BacArena: Individual-based metabolic modeling of heterogeneous microbes in complex communities. *PLoS Comput. Biol.* **13**, (2017).
10. Bauer, E. & Thiele, I. From metagenomic data to personalized in silico microbiotas : predicting dietary supplements for Crohn ' s disease. *NPJ Syst. Biol. Appl.* **4**, (2018).
11. Mukhopadhya, I. & Louis, P. Gut microbiota-derived short-chain fatty acids and their role in human health and disease. *Nature Reviews Microbiology* vol. 23 Preprint at https://doi.org/10.1038/s41579-025-01183-w (2025).
12. Quinn-Bohmann, N. *et al.* Microbial community-scale metabolic modelling predicts personalized short-chain fatty acid production profiles in the human gut. *Nat. Microbiol.* **9**, 1700–1712 (2024).

13. Best, L. *et al.* Metabolic modelling reveals the aging-associated decline of host–microbiome metabolic interactions in mice. *Nat. Microbiol.* **10**, 973–991 (2025).
14. Marinos, G., Zimmermann, J., Taubenheim, J. & Kaleta, C. Virtual Colon: Spatiotemporal modelling of metabolic interactions in a computational colonic environment. Preprint at https://doi.org/10.1101/2024.06.11.598488 (2024).
15. Versluis, D. M. *et al.* A Multiscale Spatiotemporal Model Including a Switch from Aerobic to Anaerobic Metabolism Reproduces Succession in the Early Infant Gut Microbiota. *mSystems* **7**, (2022).
16. Geng, J., Boyang, J., Li, G., López-Isunza, F. & Nielsen, J. CODY enables quantitatively spatiotemporal predictions on in vivo gut microbial variability induced by diet intervention. *Syst. Biol. (Stevenage).* **118**, (2021).
17. Javad, A.-D., Andrew, D., Amin, V. & K, M. M. R. MetaBiome: a multiscale model integrating agent-based and metabolic networks to reveal spatial regulation in gut mucosal microbial communities. *mSystems* **10**, e01652-24 (2025).
18. Chan, Friedman, Wu & Maranas. Predicting the Longitudinally and Radially Varying Gut Microbiota Composition Using Multi-Scale Microbial Metabolic Modeling. *Processes* **7**, 394 (2019).
19. Plata, G. *et al.* Growth promotion and antibiotic induced metabolic shifts in the chicken gut microbiome. *Commun. Biol.* **5**, (2022).
20. Utkina, I., Fan, Y., Willing, B. P. & Parkinson, J. Metabolic modeling of microbial communities in the chicken ceca reveals a landscape of competition and co-operation. *Microbiome* **13**, 248 (2025).
21. Al-Nijir, M., Chuck, C. J., Bedford, M. R. & Henk, D. A. Metabolic modelling uncovers the complex interplay between fungal probiotics, poultry microbiomes, and diet. *Microbiome* **12**, (2024).
22. Taverniti, V. *et al.* Probiotics Modulate Mouse Gut Microbiota and Influence Intestinal Immune and Serotonergic Gene Expression in a Site-Specific Fashion. *Front. Microbiol.* **12**, (2021).
23. Jensen, B. A. H. *et al.* Small intestine vs. colon ecology and physiology: Why it matters in probiotic administration. *Cell Reports Medicine* vol. 4 Preprint at https://doi.org/10.1016/j.xcrm.2023.101190 (2023).
24. Borda-Molina, D. *et al.* Caeca Microbial Variation in Broiler Chickens as a Result of Dietary Combinations Using Two Cereal Types, Supplementation of Crude Protein and Sodium Butyrate. *Front. Microbiol.* **11**, (2021).

908 25. Kim, E. *et al.* The flow of non-starch polysaccharides along the gastrointestinal tract of
909 broiler chickens fed either a wheat- or maize-based diet. *Animal Nutrition* **9**, (2022).
910 26. Nguyen, H. T., Bedford, M. R., Wu, S. B. & Morgan, N. K. Soluble non-starch
911 polysaccharide modulates broiler gastrointestinal tract environment. *Poult. Sci.* **100**,
912 (2021).
913 27. Glendinning, L., Stewart, R. D., Pallen, M. J., Watson, K. A. & Watson, M. Assembly
914 of hundreds of novel bacterial genomes from the chicken caecum. *Genome Biol.* **21**, 1–
915 16 (2020).
916 28. Feng, Y. *et al.* Metagenome-assembled genomes and gene catalog from the chicken gut
917 microbiome aid in deciphering antibiotic resistomes. *Commun. Biol.* **4**, (2021).
918 29. Zhang, Y. *et al.* Improved microbial genomes and gene catalog of the chicken gut from
919 metagenomic sequencing of high-fidelity long reads. *Gigascience* **11**, (2022).
920 30. Zimmermann, J., Kaleta, C. & Waschina, S. gapseq: informed prediction of bacterial
921 metabolic pathways and reconstruction of accurate metabolic models. *Genome Biol.* **22**,
922 (2021).
923 31. Rodrigues, I. & Choct, M. The foregut and its manipulation via feeding practices in the
924 chicken. *Poult. Sci.* **97**, 3188–3206 (2018).
925 32. Duve, L. R., Steenfeldt, S., Thodberg, K. & Nielsen, B. L. Splitting the scotoperiod:
926 Effects on feeding behaviour, intestinal fill and digestive transit time in broiler chickens.
927 *Br. Poult. Sci.* **52**, (2011).
928 33. Rios-Covian, D., Gueimonde, M., Duncan, S. H., Flint, H. J. & De Los Reyes-Gavilan,
929 C. G. Enhanced butyrate formation by cross-feeding between Faecalibacterium
930 prausnitzii and Bifidobacterium adolescentis. *FEMS Microbiol. Lett.* **362**, (2015).
931 34. Louis, P. & Flint, H. J. Diversity, metabolism and microbial ecology of butyrate-
932 producing bacteria from the human large intestine. *FEMS Microbiol. Lett.* **294**, (2009).
933 35. Iwami, Y., Abbe, K., Takahashi-Abbe, S. & Yamada, T. Acid production by streptococci
934 growing at low pH in a chemostat under anaerobic conditions. *Oral Microbiol. Immunol.*
935 **7**, (1992).
936 36. Carlsson, J. & Griffith, C. J. Fermentation products and bacterial yields in glucose-
937 limited and nitrogen-limited cultures of streptococci. *Arch. Oral Biol.* **19**, (1974).
938 37. SHOCKMAN, G. D. The acetate requirement of Streptococcus faecalis. *J. Bacteriol.*
939 **72**, (1956).

38. Beelen, P., Hoeven, J. S., Jong, M. H. & Hoogendoorn, H. The effect of oxygen on the growth and acid production of Streptococcus mutans and Streptococcus sanguis . *FEMS Microbiol. Lett.* **38**, (1986).
39. Shin, J. H. *et al.* Bacteroides and related species: The keystone taxa of the human gut microbiota. *Anaerobe* vol. 85 Preprint at https://doi.org/10.1016/j.anaerobe.2024.102819 (2024).
40. Lyte, J. M. *et al.* Inclusion of trans-cinnamaldehyde and caprylic acid in feed results in detectable concentrations in the chicken gut and reduces foodborne pathogen carriage. *Poult. Sci.* **103**, (2024).
41. Ge, S. *et al.* GABA regulates synaptic integration of newly generated neurons in the adult brain. *Nature* **439**, (2006).
42. Allaband, C. *et al.* Time of sample collection is critical for the replicability of microbiome analyses. *Nature Metabolism* vol. 6 1282–1293 Preprint at https://doi.org/10.1038/s42255-024-01064-1 (2024).
43. Leiber, F. *et al.* Effects of riboflavin supplementation level on health, performance, and fertility of organic broiler parent stock and their chicks. *Animal* **16**, (2022).
44. Biswas, A., Mohan, N., Dev, K., Mir, N. A. & Tiwari, A. K. Effect of dietary mannan oligosaccharides and fructo-oligosaccharides on physico-chemical indices, antioxidant and oxidative stability of broiler chicken meat. *Sci. Rep.* **11**, (2021).
45. Jahan, A. A., González Ortiz, G., Moss, A. F., Bhuiyan, M. M. & Morgan, N. K. Role of supplemental oligosaccharides in poultry diets. *World's Poultry Science Journal* vol. 78 Preprint at https://doi.org/10.1080/00439339.2022.2067805 (2022).
46. Tejeda, O. J. & Kim, W. K. Role of dietary fiber in poultry nutrition. *Animals* vol. 11 Preprint at https://doi.org/10.3390/ani11020461 (2021).
47. Hetland, H., Choct, M. & Svihus, B. Role of insoluble non-starch polysaccharides in poultry nutrition. in *World's Poultry Science Journal* vol. 60 (2004).
48. Froidurot, A. & Julliand, V. Cellulolytic bacteria in the large intestine of mammals. *Gut Microbes* vol. 14 Preprint at https://doi.org/10.1080/19490976.2022.2031694 (2022).
49. Bell, S. C. & Turner, J. M. Bacterial catabolism of threonine. Threonine degradation initiated by L-threonine hydrolyase (deaminating) in a species of Corynebacterium. *Biochemical Journal* **164**, (1977).
50. Bell, S. C. & Turner, J. M. Bacterial catabolism of threonine. Threonine degradation initiated by L-threonine acetaldehyde-lyase (aldolase) in species of Pseudomonas. *Biochemical Journal* **166**, (1977).

974 51. Simanshu, D. K., Chittori, S., Savithri, H. S. & Murthy, M. R. N. Structure and function
975 of enzymes involved in the anaerobic degradation of L-threonine to propionate. *Journal*
976 *of Biosciences* vol. 32 Preprint at https://doi.org/10.1007/s12038-007-0121-1 (2007).
977 52. Quinn-Bohmann, N. *et al.* Microbial community-scale metabolic modeling predicts
978 personalized short chain fatty acid production profiles in the human gut. *bioRxiv* Preprint
979 at https://doi.org/10.1101/2023.02.28.530516 (2023).
980 53. Zimmermann-Kogadeeva, M., Bencivenga-Barry, N. A., Zimmermann, M., Bork, P. &
981 Goodman, A. L. Multiomics and quantitative modelling disentangle diet, host, and
982 microbiota contributions to the host metabolome. *bioRxiv* 2022.08.15.503927 (2022)
983 doi:10.1101/2022.08.15.503927.
984 54. Carr, A. V., Baliga, N. S., Diener, C. & Gibbons, S. M. Personalized Clostridioides
985 difficile colonization risk prediction and probiotic therapy assessment in the human gut.
986 *Cell Syst.* **16**, 101367 (2025).
987 55. Bolyen, E. *et al.* Reproducible, interactive, scalable and extensible microbiome data
988 science using QIIME 2. *Nature Biotechnology* vol. 37 Preprint at
989 https://doi.org/10.1038/s41587-019-0209-9 (2019).
990 56. Kaehler, B. D. *et al.* Species abundance information improves sequence taxonomy
991 classification accuracy. *Nat. Commun.* **10**, (2019).
992 57. O'Leary, N. A. *et al.* Reference sequence (RefSeq) database at NCBI: Current status,
993 taxonomic expansion, and functional annotation. *Nucleic Acids Res.* **44**, (2016).
994 58. Caporaso, J. G. *et al.* QIIME allows analysis of high-throughput community sequencing
995 data. *Nature Methods* vol. 7 Preprint at https://doi.org/10.1038/nmeth.f.303 (2010).
996 59. Pang, Z. *et al.* MetaboAnalyst 5.0: Narrowing the gap between raw spectra and
997 functional insights. *Nucleic Acids Res.* **49**, (2021).
998 60. Douglas, G. M. *et al.* PICRUSt2 for prediction of metagenome functions. *Nature*
999 *Biotechnology* vol. 38 Preprint at https://doi.org/10.1038/s41587-020-0548-6 (2020).
1000 61. Gurbich, T. A. *et al.* MGnify Genomes: A Resource for Biome-specific Microbial
1001 Genome Catalogues: MGnify biome-specific genome catalogues. *J. Mol. Biol.* **435**,
1002 (2023).
1003 62. Guenter, W. & Sell, J. L. Magnesium absorption and secretion along the gastrointestinal
1004 tract of the chicken. *J. Nutr.* **103**, (1973).
1005 63. David, L. S., Abdollahi, M. R., Ravindran, G., Walk, C. L. & Ravindran, V. Studies on
1006 the measurement of ileal calcium digestibility of calcium sources in broiler chickens.
1007 *Poult. Sci.* **98**, (2019).

1008 64. Haetinger, V. S. *et al.* Ileal phosphorus digestibility of soybean meal for broiler chickens
1009 remains consistent across institutions in a collaborative study regardless of non-phytate
1010 phosphorus concentration in the pre-experimental starter diet. *Poult. Sci.* **103**, (2024).
1011 65. Mutucumarana, R. K., Ravindran, V., Ravindran, G. & Cowieson, A. J. Measurement
1012 of true ileal digestibility and total tract retention of phosphorus in corn and canola meal
1013 for broiler chickens. *Poult. Sci.* **93**, (2014).
1014 66. Chang'a, E. P. *et al.* Energy utilization, nutrient digestibility and bone quality of broiler
1015 chickens fed Tanzania-type diets in different forms with enzymes. *J. Anim. Sci. Technol.*
1016 **61**, (2019).
1017 67. Thomas, D. V. & Ravindran, V. Mineral retention in young broiler chicks fed diets based
1018 on wheat, Sorghum or maize. *Asian-Australas. J. Anim. Sci.* **23**, (2010).
1019 68. Ward, T. L., Watkins, K. L. & Southern, L. L. Interactive effects of dietary copper, water
1020 copper, and Eimeria spp. infection on growth, water intake, and plasma and liver copper
1021 concentrations of poults. *Poult. Sci.* **74**, (1995).
1022 69. Macelline, S. P., Chrystal, P. V., Selle, P. H. & Liu, S. Y. Protein sources and starch-
1023 protein digestive dynamics manipulate growth performance in broiler chickens defined
1024 by an equilateral-triangle response surface design. *Animal Nutrition* **9**, (2022).
1025 70. Stefanello, C. *et al.* Starch digestibility, energy utilization, and growth performance of
1026 broilers fed corn-soybean basal diets supplemented with enzymes. *Poult. Sci.* **94**, (2015).
1027 71. Khalil, M. M., Abdollahi, M. R., Zaefarian, F. & Ravindran, V. Measurement of ileal
1028 endogenous energy losses and true ileal digestible energy of cereal grains for broiler
1029 chickens. *Poult. Sci.* **99**, (2020).
1030 72. Truong, H. H., Chrystal, P. V., Moss, A. F., Selle, P. H. & Liu, S. Y. Rapid protein
1031 disappearance rates along the small intestine advantage poultry performance and
1032 influence the post-enteral availability of amino acids. *British Journal of Nutrition* **118**,
1033 (2017).
1034 73. Tancharoenrat, P., Ravindran, V., Zaefarian, F. & Ravindran, G. Digestion of fat and
1035 fatty acids along the gastrointestinal tract of broiler chickens. *Poult. Sci.* **93**, 371–379
1036 (2014).
1037
1038
1039
1040
1041

1049 **SUPPLEMENTAL MATERIAL**

1050 **Supplementary Figure 1. Taxonomic composition of gut microbiota in different gut**
1051 **compartments.** The relative abundance of bacterial families derived from 16S rRNA survey
1052 data is shown for samples from the gizzard, duodenum, jejunum, ileum, cecum, and colon,
1053 separated by corn and wheat diets. Color bars represent different taxonomic families, with
1054 relative proportions depicted for each gut compartment.

1055 **Supplementary Figure 2. Distribution of enzyme commission numbers (ECs) across**
1056 **metabolic models.** The columns of the heatmap represent individual ECs, while the rows
1057 correspond to metabolic models representing different taxa. ECs are annotated using KEGG
1058 pathway designations, indicated in two layers to reflect primary and secondary pathway
1059 associations. For ECs lacking KEGG pathway annotation, MetaCyc pathway annotation was
1060 utilized when available. For ECs mapped to 3 or more major pathway categories, "Multiple
1061 superpathways" category was assigned. Each row represents a different taxon, annotated by
1062 taxonomic family.
1063
1064 **Supplementary Figure 3. Reaction-level drivers of compartmental separation observed**
1065 **in Figure 1E. A.** Distribution of PC1 (left) and PC2 (right) scores from the principal
1066 coordinates analysis (PCoA shown in **Figure 1E**) across gut compartments. PCoA was
1067 performed on Bray-Curtis dissimilarities of community metabolic reaction profiles weighted
1068 by species relative abundances. PC scores reflect the relative contribution of reaction sets
1069 associated with each axis rather than distances to compartment centroids. Dashed red lines
1070 indicate zero for each axis. PC1 primarily separates upper gastrointestinal tract compartments
1071 (gizzard, duodenum, jejunum, ileum) from lower gut compartments (cecum, colon), whereas
1072 PC2 captures additional metabolic stratification along the proximal-distal axis. **B.** Heatmap
1073 showing mean compartment-level abundances of metabolic reactions most strongly associated
1074 with PC1 and PC2 in Fig. 1E. Reactions were selected based on the highest positive and
1075 negative Spearman correlations between individual reaction abundances and PCoA axis scores
1076 (top loadings). Values are column-scaled (z-scores per reaction) to emphasize relative
1077 enrichment across compartments. Reactions associated with positive PC1 scores (upper GIT)
1078 include bile salt hydrolases, membrane lipid synthesis pathways, and fatty acid biosynthesis,
1079 consistent with biosynthetically active, oxygen-replete environments. In contrast, reactions
1080 associated with negative PC1 scores (lower GIT) are enriched for anaerobic fermentation
1081 processes, including short-chain fatty acid biosynthesis, polysaccharide degradation, and
1082 amino acid fermentation.
1083
1084 **Supplementary Figure 4. PCoA of metabolite concentrations after 96-hour simulations.**
1085 All 10 samples from corn-fed and wheat-fed chickens are shown, comparing control conditions
1086 (black dots) with various dietary supplements across all six gut compartments. Top panels:
1087 PCoA based on all metabolite concentrations. Bottom panels: PCoA based solely on SCFA
1088 concentrations. Supplement types are indicated by symbols and colors, with dosing shown after
1089 underscores (e.g., Inulin_2 = 2g per 100g diet).
1090
1091 **Supplementary Figure 5. SCFA production rates in simulations with supplementation.**
1092 Fold changes in total SCFA production by the microbial community over 96 hours of
1093 simulation when supplemented with a specific compound (y-axis), compared to the control, in
1094 ileum and cecum. The y-axis lists the various dietary supplements tested, with their
1095 concentrations indicated after the underscore (e.g., Inulin_2 denotes supplementation with 2g
1096 per 100g of diet). Each dot represents a fold change in community flux in a replicate (n=5) of

a sample (n=10). Significance based on two-sided Wilcoxon signed-rank test with Benjamini–Hochberg correction for multiple testing: * – pvalue- adjusted < 0.05, ** – pvalue-adjusted < 0.01, *** – pvalue-adjusted < 0.001.

Supplementary Figure 6. Taxonomic composition of gut microbiota in trial-derived samples from ileum and cecum gut compartments. The relative abundances of bacterial families are derived from 16S rRNA survey data. Color bars represent different taxonomic families, with relative proportions depicted for each gut compartment.

Supplementary Figure 7. Experimental validation of metabolite concentrations in response to dietary supplementation. Targeted metabolomics measurements from chicken ileum and cecum samples following 7-day dietary supplementation. **A**. Box plots showing metabolite concentrations (μmol/g dry weight) across treatment groups for both ileum and cecum compartments. Each metabolite panel displays individual data points overlaid on box plots, with Kruskal-Wallis (KW) p-values shown in the top-left of each facet. Significant pairwise comparisons between treatment groups and control (determined by Dunn's post-hoc test with Benjamini-Hochberg correction) are indicated by brackets with asterisks. **B**. Bar plots showing log2 fold changes relative to control group for each treatment in ileum and cecum. Asterisks indicate statistical significance from two-sample Wilcoxon rank-sum tests with Benjamini-Hochberg correction (* - $p < 0.05$, ** - $p < 0.01$, *** - $p < 0.001$). Fumarate showed consistent depletion across all treatments (KW p=0.002), contrasting with model predictions of net microbial production, suggesting rapid consumption or host absorption. Butyrate exhibited significant treatment effects (KW p=0.029), with increases under low-dose cellulose and starch aligning with predicted production by Ruminococcaceae, Butyricicoccaceae, and Lachnospiraceae. Lactate showed significant treatment effects (KW p=0.034) with high inter-individual variability, consistent with its role as both a fermentation product and rapidly consumed substrate. Succinate showed predominantly negative fold changes despite model predictions of increased production under starch (Bacteroidaceae) and cellulose (Lachnospiraceae), indicating additional metabolic sinks not captured in models. Acetate production increased in ileum, especially under cellulose and L-threonine treatments, however no consistent treatment effects were observed in cecum, reflecting acetate broad production across multiple families.

Supplementary Figure 8. Predicted taxonomic contributions to metabolite production in the trial-informed 2-compartment model. Bacterial flux predictions from 48-hour simulations of the trial-informed 2-compartment (ileum-cecum) model showing which taxonomic families contribute to production of seven fermentation metabolites. Horizontal stacked bar plots display cumulative metabolic flux (fmol/gdW/hour) for acetate, propionate, butyrate, lactate, fumarate, succinate, and alpha-ketoglutarate across all seven treatment groups (G1 (control), G2 (cellulose 2g/100g), G3 (cellulose 8g/100g), G4 (L-threonine 1g/100g), G5 (L-threonine 5g/100g), G6 (starch 5g/100g), and G7 (starch 10g/100g)) in ileum and cecum compartments. Each color represents a taxonomic family. Flux values represent total community production summed across all 48 hours of simulation and normalized by community size. The figure illustrates predicted treatment-specific modulation of bacterial metabolism, with cellulose and starch supplementation enhancing butyrate production capacity in cellulose- and starch-fermenting families, as referenced in the main text analyses.

Supplementary Table S1. MAG selections for 29 bacterial species in the multi-compartment metabolic model. Genome assignments for 29 bacterial species selected for genome-scale metabolic modeling of chicken gastrointestinal tract compartments. Species

represent prevalent taxa from day 10 post-hatch samples across six GIT sites. Table includes species names, MAG identifiers, genome source databases (Intestinal Microbial Genomes ANI99 collection, HoloFood chicken gut MAG catalog), match quality categories, CheckM quality metrics (completeness, contamination), originating GIT site, assembly type, complete taxonomic classification, and selection notes. NCBI reference genomes were used when high-quality matches were unavailable in the three chicken gut MAG databases used as a reference.

Supplementary Table S2. Parameters for spatial metabolic simulations using BacArena. A. Simulation parameters for the 6-compartment model. Parameters for spatial metabolic simulations using BacArena. Table S2A provides parameters for the six-compartment gastrointestinal tract model representing gizzard, duodenum, jejunum, ileum, cecum, and colon. Parameters include initial bacterial community sizes per compartment, spatial grid dimensions (arena size), basal nutrient availability (essential metabolite concentrations), physicochemical conditions (pH, oxygen concentration), and dietary input schedules (proportion and timing of feed addition to gizzard). Additional parameters specify differential removal rates for day versus night periods and substrate-level removal percentages, reflecting circadian feeding patterns and intestinal motility in broiler chickens. **B. Simulation parameters for the ileum-cecum model.** Table S2B provides parameters for the simplified two-compartment ileum-cecum model, including bacterial removal rates and frequencies that simulate digesta flow and GIT transit. Additional parameters specify differential removal rates for day versus night periods and substrate-level removal percentages, reflecting circadian feeding patterns and intestinal motility in broiler chickens.

Supplementary Table S3. MAG assignments for metabolic models in ileal and cecal microbial communities. Representative MAG assignments for 267 functionally clustered ASVs from paired chicken ileum and cecum samples (validation trial). ASVs were clustered by 75% functional similarity (Jaccard index) of PICRUSt2-predicted enzyme profiles, with representatives selected to maximize MAG coverage. MAGs were selected from three chicken gut databases: ANI99 collection (Huang et al. 2022), MGnify chicken gut catalog (13,389 genomes), and HoloFood 12k MAG catalog. Selection prioritized combined BLAST quality (identity, bit score) and genome quality (completeness, contamination). Table includes: sample identifiers, treatment groups (control vs. prebiotic), body site (ileum/cecum), cumulative relative abundance per functional cluster, MAG identifiers, genome source databases, BLAST statistics (identity, bit score), MAG quality metrics (completeness, contamination), match quality categories (excellent/good/acceptable), and full taxonomic classifications.

Supplementary Table S4. Diet compositions for metabolic simulations. Complete metabolic compositions of corn-based and wheat-based grower diets used in simulations. Feed compositions from the original trial were translated into corresponding metabolites using animal feed tables mapping nutrient content to feed items. Oil compositions were sourced from vmh.life. Sugar and fiber categories were resolved into specific carbohydrates and polysaccharides based on published compositional studies, with cellulose used as the primary fiber source.

Supplementary Table S5. Reactions added to and removed from metabolic models based on CAZyme gene annotations. Manual curation of metabolic reactions to improve representation of complex carbohydrate metabolism beyond gapseq's default modelSEED database. Sheet 1 documents 55 reactions added based on CAZymes detected by dbCAN3 analysis. Reactions were incorporated directly from modelSEED when exact matches existed, or manually defined using multiple biochemical databases for enzymes not in modelSEED.

Includes polysaccharide degradation reactions (arabinan, xyloglucan, xylan, etc.) and associated transport reactions, with detailed information on reaction definitions, EC numbers, stoichiometry, reversibility, affected species models, and newly introduced metabolites with chemical formulas. Sheet 2 documents 14 reactions removed from models when both: (1) the corresponding CAZyme was not detected by dbCAN3 in the genome, and (2) no significant sequence similarity was found during gapseq reaction search. Removed reactions include incorrectly predicted fructan biosynthesis and starch degradation activities.